

# Simulations of population balance systems with one internal coordinate using finite element methods

Volker John<sup>a,\*</sup>, Teodora Mitkova<sup>b</sup>, Michael Roland<sup>a</sup>, Kai Sundmacher<sup>c,d</sup>, Lutz Tobiska<sup>e</sup>, Andreas Voigt<sup>d</sup>

<sup>a</sup>FR 6.1 – Mathematik, Universität des Saarlandes, Postfach 15 11 50, 66041 Saarbrücken, Germany

<sup>b</sup>Institute of Mathematics, University of Basel, Rheinsprung 21, 4051 Basel, Switzerland

<sup>c</sup>Max Planck Institute for Dynamics of Complex Technical Systems, Sandtorstr. 1, 39106 Magdeburg, Germany

<sup>d</sup>Otto-von-Guericke-Universität, Process Systems Engineering, PSF 4120, 39016 Magdeburg, Germany

<sup>e</sup>Institut für Analysis und Numerik, PF 4120, Otto-von-Guericke-Universität Magdeburg, 39106 Magdeburg, Germany

## ARTICLE INFO

### Article history:

Received 12 November 2007

Received in revised form 4 March 2008

Accepted 5 May 2008

Available online 15 May 2008

### Keywords:

Population balance systems

Calcium carbonate precipitation

Navier–Stokes equations

Convection–diffusion–reaction equations

Finite element methods

## ABSTRACT

The paper presents an approach for simulating a precipitation process which is described by a population balance system consisting of the incompressible Navier–Stokes equations, nonlinear convection–diffusion–reaction equations and a transport equation for the particle size distribution (PSD). The Navier–Stokes equations and the convection–diffusion–reaction equations are discretized implicitly in time and with finite element methods in space. Two stabilization techniques for the convection–diffusion–reaction equations are investigated. An explicit temporal discretization and an upwind finite difference method are used for discretizing the equation of the PSD. Simulations of the calcium carbonate precipitation in a cavity are presented which study the influence of the flow field on the PSD at the outflow. It is shown that variations of the positions of the inlets change the volume fraction of the PSD at the center of the outlet. The corresponding medians of the volume fraction differ up to a factor of about three. In addition, it is demonstrated that the use of the two different stabilized finite element methods for the convection–diffusion–reaction equations leads to completely different numerical results.

© 2008 Elsevier Ltd. All rights reserved.

## 1. Introduction

Many industrial chemical processes deal with the production of particulate products using wet chemistry. In particular, precipitations are widely used to produce particles with prescribed properties. The numerical simulation of precipitation processes is of high interest in order to obtain a better understanding of these processes, to improve their control and finally to optimize them.

Precipitation processes are modeled by population balance systems consisting of equations describing the flow field (Navier–Stokes equations), equations for the chemical reaction (convection–diffusion–reaction equations) and an equation for the particle size distribution (PSD, transport equation). Besides the coupling of these equations, the main difficulty in simulations is that the PSD depends not only on time and space but also on properties

of the particles (internal coordinates). Consequently, the equation for the PSD is given in a higher dimensional domain than the other equations.

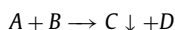
There are several approaches for circumventing this dimensional curse of the PSD equation. The assumption of an ideal mixing of all substances leads to the independence of the PSD of the space variables, see for instance Heineken et al. (2007). The method of moments (MOM) and improved versions like QMOM or DQMOM (Marchisio and Fox, 2005) replace the equation of the PSD by a coupled system of equations given in the same dimension as the other equations. However, instead of the PSD, only the first few moments of the PSD are computed. The reconstruction of a function from a finite number of its moments is a severely ill-posed problem and a recent review (John et al., 2007) shows that reliable algorithms for solving this problem are in general not available.

We think that in future the simulation of the coupled population balance system will become necessary for obtaining reliable results. First efforts in this direction can be found in (Kulikov et al., 2005, 2007; Schwarzer et al., 2006; Gradl et al., 2007). Also our work is directed towards the efficient solution of these systems and first steps are presented here.

\* Corresponding author. Tel.: +49 681 302 4445.

E-mail addresses: [john@math.uni-sb.de](mailto:john@math.uni-sb.de) (V. John), [Teodora.Mitkova@unibas.ch](mailto:Teodora.Mitkova@unibas.ch) (T. Mitkova), [roland@math.uni-sb.de](mailto:roland@math.uni-sb.de) (M. Roland), [sundmacher@mpi-magdeburg.mpg.de](mailto:sundmacher@mpi-magdeburg.mpg.de) (K. Sundmacher), [lutz.tobiska@mathematik.uni-magdeburg.de](mailto:lutz.tobiska@mathematik.uni-magdeburg.de) (L. Tobiska), [voigt@mpi-magdeburg.mpg.de](mailto:voigt@mpi-magdeburg.mpg.de) (A. Voigt).

A precipitation process considers a chemical reaction of the form



in a liquid phase where the initially dissolved product  $C$  starts to precipitate if its local concentration exceeds the saturation concentration. Of primary interest in applications is the PSD of the solid phase of the product  $C$ .

This paper describes a numerical approach for the simulation of a population balance system which models the calcium carbonate precipitation in a cavity with the following modeling assumptions:

- the background flow is two-dimensional, incompressible and laminar;
- the chemical reaction is isothermal;
- the PSD depends on one internal coordinate, namely the size of the particles;
- the particles, resp. the PSD, do not affect the flow field since their concentration is small;
- the particles follow the streamlines of the flow field because of their small size; and
- nucleation and growth of particles, which are the most important phenomena governing the process of particle precipitation, are included into the model; agglomeration and breakage of particles are neglected.

From these assumptions, it follows that the flow field can be simulated independently of the chemical reaction and the precipitation process.

There are many different numerical methods for solving the individual equations in the coupled population balance system. However, which methods should be used is not clear and there are many open questions concerning the efficient application of possible candidates in the coupled system. Simplifying assumptions, like the consideration of a two-dimensional laminar flow, should facilitate the assessment of numerical methods.

This paper presents simulations of population balance systems describing calcium carbonate precipitations in a cavity. The discretization of the equations in these systems is based mainly on implicit time stepping schemes and finite element methods. Two standard stabilization techniques will be explored in the finite element discretization of the convection–diffusion–reaction equations. One of them leads generally to smeared solutions without spurious oscillations, whereas the other one is less smearing but exhibits spurious oscillations in the solutions.

The numerical investigations study the influence of different in-flow positions on the PSD at the outflow. In addition, it will be demonstrated that the two finite element stabilization techniques of the convection–diffusion–reaction equations lead to very different results in the simulation of the precipitation process.

## 2. The population balance system for the precipitation process

Incompressible flows are governed by the incompressible Navier–Stokes equations

$$\frac{\partial \tilde{\mathbf{u}}}{\partial \tilde{t}} - \nu \Delta \tilde{\mathbf{u}} + (\tilde{\mathbf{u}} \cdot \nabla) \tilde{\mathbf{u}} + \frac{1}{\rho} \nabla \tilde{p} = \mathbf{0} \quad \text{in } (0, \tilde{T}] \times \tilde{\Omega},$$

$$\nabla \cdot \tilde{\mathbf{u}} = 0 \quad \text{in } [0, \tilde{T}] \times \tilde{\Omega},$$

where  $\tilde{\mathbf{u}}$  [m/s] denotes the fluid velocity,  $\tilde{p}$  [kg/(m s<sup>2</sup>)] the pressure,  $\nu$  [m<sup>2</sup>/s] and  $\rho$  [kg/m<sup>3</sup>] the kinematic viscosity and the density, respectively,  $\tilde{\Omega}$  is the flow domain and  $\tilde{T}$  is the final time.

Let  $\tilde{c}_i$  [kmol/m<sup>3</sup>],  $i \in \{A, B, C\}$ , denote the concentration of the dissolved substances  $A$ ,  $B$  and  $C$ , respectively. The behavior of

the reactants  $A$  and  $B$  can be described by a system of scalar convection–diffusion–reaction equations for  $\tilde{c}_i$ ,  $i \in \{A, B\}$ ,

$$\frac{\partial \tilde{c}_i}{\partial \tilde{t}} - D_i \Delta \tilde{c}_i + \tilde{\mathbf{u}} \cdot \nabla \tilde{c}_i + \tilde{r}_{\text{chem}}(\tilde{c}_A, \tilde{c}_B) = 0 \quad \text{in } (0, \tilde{T}] \times \tilde{\Omega}.$$

Here,  $D_i$  [m<sup>2</sup>/s] denotes the diffusion coefficient of  $A$  and  $B$ . The rate of the chemical reaction  $\tilde{r}_{\text{chem}}(\tilde{c}_A, \tilde{c}_B)$  [kmol/(m<sup>3</sup> s)] is given by

$$\tilde{r}_{\text{chem}}(\tilde{c}_A, \tilde{c}_B) = k_R \tilde{c}_A \tilde{c}_B,$$

with the rate constant  $k_R$  [m<sup>3</sup>/(kmol s)]. The equation of the product  $C$  has the form

$$\frac{\partial \tilde{c}_C}{\partial \tilde{t}} - D_C \Delta \tilde{c}_C + \tilde{\mathbf{u}} \cdot \nabla \tilde{c}_C - \tilde{r}_{\text{chem}}(\tilde{c}_A, \tilde{c}_B) + \tilde{r}_{\text{nuc}}(\tilde{c}_C) + \tilde{r}_g(\tilde{c}_C, \tilde{f}) = 0 \quad \text{in } (0, \tilde{T}] \times \tilde{\Omega},$$

with the diffusion coefficient  $D_C$  [m<sup>2</sup>/s]. The rate of decrease of  $\tilde{c}_C$  due to the nucleation  $\tilde{r}_{\text{nuc}}(\tilde{c}_C)$  [kmol/(m<sup>3</sup> s)] is given by

$$\tilde{r}_{\text{nuc}}(\tilde{c}_C) = C_{\text{nuc}} \tilde{d}_{p,0}^3 \tilde{B}_{\text{nuc}}(\tilde{c}_C),$$

where  $C_{\text{nuc}}$  [kmol/m<sup>3</sup>] denotes a model nucleation constant,  $\tilde{d}_{p,0}$  [m] the smallest particle diameter (the nuclei size) and the nucleation rate  $\tilde{B}_{\text{nuc}}(\tilde{c}_C)$  [1/(m<sup>3</sup> s)] is modeled by (Ramkrishna, 2000)

$$\tilde{B}_{\text{nuc}}(\tilde{c}_C) = \begin{cases} k_{\text{nuc}} \left( \tilde{c}_C - c_{C,\infty}^{\text{sat}} \exp \left( \frac{C_2}{\tilde{d}_{p,0}} \right) \right)^5 & \text{if } \tilde{c}_C > c_{C,\infty}^{\text{sat}} \exp \left( \frac{C_2}{\tilde{d}_{p,0}} \right), \\ 0 & \text{else.} \end{cases}$$

Here,  $k_{\text{nuc}}$  [(1/(m<sup>3</sup> s))/(kmol/m<sup>3</sup>)<sup>5</sup>] is the nucleation constant,  $c_{C,\infty}^{\text{sat}}$  [kmol/m<sup>3</sup>] is the saturation concentration of the product  $C$  and  $C_2$  [m] is a model constant. The rate of decrease of  $\tilde{c}_C$  due to the growth of the particles  $\tilde{r}_g(\tilde{c}_C, \tilde{f})$  [kmol/(m<sup>3</sup> s)] is expressed by

$$\tilde{r}_g(\tilde{c}_C, \tilde{f}) = C_G \int_{\tilde{d}_{p,0}}^{\tilde{d}_{p,\max}} \tilde{G}(\tilde{c}_C) \tilde{d}_p^2 \tilde{f} d(\tilde{d}_p),$$

where  $C_G$  [kmol/m<sup>3</sup>] denotes a model growth constant,  $\tilde{d}_{p,\max}$  [m] is an upper bound for the particle diameter,  $\tilde{d}_p$  [m] is the particle diameter and  $\tilde{f}(\tilde{t}, \tilde{\mathbf{x}}, \tilde{d}_p)$  [1/m<sup>4</sup>] is the PSD. The growth rate  $\tilde{G}(\tilde{c}_C)$  [m/s] is considered to be independent of the size of the particles and, similar as in Heineken et al. (2007), it is given by

$$\tilde{G}(\tilde{c}_C) = k_G (\tilde{c}_C - c_{C,\infty}^{\text{sat}}),$$

where  $k_G$  [m<sup>4</sup>/(kmol s)] is the growth rate constant.

The concentration of the substance  $D$  is not simulated since it is not of interest for the precipitation process.

Finally, the equation for the PSD is given by

$$\frac{\partial \tilde{f}}{\partial \tilde{t}} + \tilde{\mathbf{u}} \cdot \nabla \tilde{f} + \tilde{G}(\tilde{c}_C) \frac{\partial \tilde{f}}{\partial \tilde{d}_p} = 0$$

in  $(0, \tilde{T}] \times \tilde{\Omega} \times (\tilde{d}_{p,0}, \tilde{d}_{p,\max})$ .

We reformulate the population balance system in dimensionless form, which will be the basis of the numerical simulations. Introducing the dimensionless variables

$$\mathbf{u} = \frac{\tilde{\mathbf{u}}}{u_\infty}, \quad p = \frac{\tilde{p}}{p_\infty}, \quad t = \frac{\tilde{t}}{t_\infty}, \quad x_i = \frac{\tilde{x}_i}{l_\infty} \quad (i = 1, 2),$$

and setting the time and pressure scales to

$$t_\infty = \frac{l_\infty}{u_\infty}, \quad p_\infty = \rho u_\infty^2,$$

one obtains the Navier–Stokes equations in dimensionless form

$$\frac{\partial \mathbf{u}}{\partial t} - \frac{1}{Re} \Delta \mathbf{u} + (\mathbf{u} \cdot \nabla) \mathbf{u} + \nabla p = \mathbf{0} \quad \text{in } (0, T] \times \Omega, \quad (1)$$

$$\nabla \cdot \mathbf{u} = 0 \quad \text{in } [0, T] \times \Omega, \quad (2)$$

where  $Re = u_\infty l_\infty / \nu$  is the Reynolds number and  $T = \tilde{T}/t_\infty$ .

Defining the dimensionless concentrations by  $c_i = \tilde{c}_i / c_\infty$ ,  $i \in \{A, B\}$ , leads to the dimensionless equations for the reactants A and B

$$\frac{\partial c_i}{\partial t} - \frac{D_i}{u_\infty l_\infty} \Delta c_i + \mathbf{u} \cdot \nabla c_i + k_R \frac{l_\infty c_\infty}{u_\infty} c_A c_B = 0, \quad (3)$$

defined in  $(0, T] \times \Omega$ .

With the dimensionless variables

$$c_C = \frac{\tilde{c}_C}{c_{C,\infty}}, \quad f = \frac{\tilde{f}}{f_\infty}, \quad d_p = \frac{\tilde{d}_p}{d_{p,\infty}}$$

and the scales

$$c_{C,\infty} = c_{C,\infty}^{\text{sat}} \exp\left(\frac{C_2}{d_{p,0}}\right), \quad d_{p,\infty} = \tilde{d}_{p,\text{max}},$$

$$f_\infty = \frac{u_\infty}{C_G k_G d_{p,\infty}^3 l_\infty},$$

the dimensionless equation for the concentration of the dissolved product C is obtained. One gets

$$\begin{aligned} \frac{\partial c_C}{\partial t} - \frac{D_C}{u_\infty l_\infty} \Delta c_C + \mathbf{u} \cdot \nabla c_C - A_{\text{chem}} c_A c_B \\ + A_{\text{nuc}} \max\{0, (c_C - 1)^5\} + \left(c_C - \frac{c_{C,\infty}^{\text{sat}}}{c_{C,\infty}}\right) \int_{d_{p,\min}}^1 d_p^2 f d(d_p) = 0 \end{aligned} \quad (4)$$

in  $(0, T] \times \Omega$ , with the constants

$$A_{\text{chem}} = k_R \frac{c_{C,\infty}^2 l_\infty}{c_{C,\infty} u_\infty}, \quad d_{p,\min} = \frac{\tilde{d}_{p,0}}{d_{p,\infty}},$$

$$A_{\text{nuc}} = C_{\text{nuc}} \tilde{d}_{p,0}^3 k_{\text{nuc}} \frac{l_\infty c_{C,\infty}^4}{u_\infty}.$$

Finally, the equation for the dimensionless PSD is given by

$$\frac{\partial f}{\partial t} + \mathbf{u} \cdot \nabla f + G(c_C) \frac{l_\infty}{d_{p,\infty}} \frac{\partial f}{\partial d_p} = 0 \quad (5)$$

in  $(0, T] \times \Omega \times (d_{p,\min}, 1)$  with

$$G(c_C) = \frac{k_G c_{C,\infty}}{u_\infty} \left(c_C - \frac{c_{C,\infty}^{\text{sat}}}{c_{C,\infty}}\right).$$

### 3. The numerical solution algorithms

The Navier–Stokes equations (1), (2) and system (3), (4) modeling the chemical reaction were discretized in time with the Crank–Nicolson scheme. This implicit temporal discretization was applied with an equidistant time step  $\Delta t$ . In each discrete time  $t_k$ , first the Navier–Stokes equations (1) and (2) were solved. After the temporal discretization, one gets the following nonlinear system

$$\begin{aligned} \mathbf{u}_k + \frac{\Delta t}{2} \left( -\frac{1}{Re} \Delta \mathbf{u}_k + (\mathbf{u}_k \cdot \nabla) \mathbf{u}_k \right) + \nabla p_k \\ = \mathbf{u}_{k-1} - \frac{\Delta t}{2} \left( -\frac{1}{Re} \Delta \mathbf{u}_{k-1} + (\mathbf{u}_{k-1} \cdot \nabla) \mathbf{u}_{k-1} \right) \quad \text{in } \Omega, \\ \nabla \cdot \mathbf{u}_k = 0 \quad \text{in } \Omega. \end{aligned}$$

This system was linearized with a simple fixed point iteration. Let  $\mathbf{u}_k^{(0)} = \mathbf{u}_{k-1}$ , compute  $\mathbf{u}_k^{(i)}$ ,  $i = 1, 2, \dots$ , by solving

$$\begin{aligned} \mathbf{u}_k^{(i)} + \frac{\Delta t}{2} \left( -\frac{1}{Re} \Delta \mathbf{u}_k^{(i)} + (\mathbf{u}_k^{(i-1)} \cdot \nabla) \mathbf{u}_k^{(i)} \right) + \nabla p_k^{(i)} \\ = \mathbf{u}_{k-1} - \frac{\Delta t}{2} \left( -\frac{1}{Re} \Delta \mathbf{u}_{k-1} + (\mathbf{u}_{k-1} \cdot \nabla) \mathbf{u}_{k-1} \right) \quad \text{in } \Omega, \end{aligned} \quad (6)$$

$$\nabla \cdot \mathbf{u}_k^{(i)} = 0 \quad \text{in } \Omega. \quad (7)$$

For discretizing the linear saddle point problems (6) and (7) in space, the inf-sup stable  $Q_2/P_1^{\text{disc}}$  finite element method (Matthies and Tobiska, 2002) was used, i.e. the velocity field is approximated with continuous, piecewise biquadratic functions and the pressure with discontinuous, linear functions. The fixed point iteration in  $t_k$  was stopped if the residual was sufficiently small. The combination of the Crank–Nicolson scheme, the simple fixed point iteration and the  $Q_2/P_1^{\text{disc}}$  finite element method has been proven to be an efficient and accurate way of simulating laminar flows (John, 2004, 2006).

After having computed the flow field in  $t_k$ , the coupled system of Eqs. (3) for  $c_A$  and  $c_B$  was solved. This nonlinear system was also linearized with a simple fixed point iteration. Using the current approximation of  $c_B$  in Eq. (3), a new approximation of  $c_A$  was computed, which in turn was used to compute a new approximation of  $c_B$ . Thus, the fixed point iteration in  $t_k$  looks as follows. Given  $c_{B,k}^{(0)} = c_{B,k-1}$ , solve

$$\begin{aligned} c_{A,k}^{(i)} + \frac{\Delta t}{2} \left( -\frac{D_A}{u_\infty l_\infty} \Delta c_{A,k}^{(i)} + \mathbf{u}_k \cdot \nabla c_{A,k}^{(i)} + k_R \frac{l_\infty c_\infty}{u_\infty} c_{B,k}^{(i-1)} c_{A,k}^{(i)} \right) \\ = c_{A,k-1} - \frac{\Delta t}{2} \left( -\frac{D_A}{u_\infty l_\infty} \Delta c_{A,k-1} + \mathbf{u}_{k-1} \cdot \nabla c_{A,k-1} \right. \\ \left. + k_R \frac{l_\infty c_\infty}{u_\infty} c_{A,k-1} c_{B,k-1} \right) \quad \text{in } \Omega, \\ c_{B,k}^{(i)} + \frac{\Delta t}{2} \left( -\frac{D_B}{u_\infty l_\infty} \Delta c_{B,k}^{(i)} + \mathbf{u}_k \cdot \nabla c_{B,k}^{(i)} + k_R \frac{l_\infty c_\infty}{u_\infty} c_{A,k}^{(i)} c_{B,k}^{(i)} \right) \\ = c_{B,k-1} - \frac{\Delta t}{2} \left( -\frac{D_B}{u_\infty l_\infty} \Delta c_{B,k-1} + \mathbf{u}_{k-1} \cdot \nabla c_{B,k-1} \right. \\ \left. + k_R \frac{l_\infty c_\infty}{u_\infty} c_{A,k-1} c_{B,k-1} \right) \quad \text{in } \Omega, \end{aligned}$$

$i = 1, 2, \dots$ . This iteration was stopped if the residual of the nonlinear system was sufficiently small.

After the computation of  $c_A$  and  $c_B$ , the concentration of the reactant C can be computed by solving Eq. (4). The nucleation term was treated explicitly, using  $c_C$  from the previous discrete time. Similarly, for evaluating the integral term in Eq. (4), we used  $c_C$  and the PSD  $f$  from the previous time step. Thus,  $c_C$  can be computed in  $t_k$  by solving the linear equation

$$\begin{aligned} c_{C,k} + \frac{\Delta t}{2} \left( -\frac{D_C}{u_\infty l_\infty} \Delta c_{C,k} + \mathbf{u}_k \cdot \nabla c_{C,k} \right) \\ = c_{C,k-1} - \frac{\Delta t}{2} \left( -\frac{D_C}{u_\infty l_\infty} \Delta c_{C,k-1} + \mathbf{u}_{k-1} \cdot \nabla c_{C,k-1} \right) \\ + \frac{\Delta t}{2} \left[ A_{\text{chem}} (c_{A,k-1} c_{B,k-1} + c_{A,k} c_{B,k}) \right. \\ \left. - A_{\text{nuc}} (\max\{0, (c_{C,k-1} - 1)^5\} + \max\{0, (c_{C,k-2} - 1)^5\}) \right. \\ \left. - \left( \left( c_{C,k-1} - \frac{c_{C,\infty}^{\text{sat}}}{c_{C,\infty}} \right) \int_{d_{p,\min}}^1 d_p^2 f_{k-1} d(d_p) \right. \right. \\ \left. \left. + \left( c_{C,k-2} - \frac{c_{C,\infty}^{\text{sat}}}{c_{C,\infty}} \right) \int_{d_{p,\min}}^1 d_p^2 f_{k-2} d(d_p) \right) \right] \quad \text{in } \Omega, \end{aligned}$$

with  $c_{C,-1} = f_{-1} := 0$ .

The (linearized) equations for the concentrations were discretized in space with the  $Q_1$  finite element, i.e. the concentrations

were approximated by continuous and piecewise bilinear functions. Since these equations are convection- and reaction-dominated, the application of a stabilized method is necessary. Using the standard Galerkin finite element method leads to numerical solutions which are globally polluted by large spurious oscillations. We investigated in the simulations two different stabilization techniques—the Samarskij upwinding scheme (Tabata, 1977) and the streamline-upwind Petrov–Galerkin (SUPG) stabilization (Hughes and Brooks, 1979; Roos et al., 1996). The latter one is one of the most popular stabilization schemes and its stabilization parameters were chosen in our simulations as proposed in Lube and Rapin (2006).

The Samarskij upwinding scheme treats the convective term similar to a finite difference or finite volume upwind method. This scheme applied to steady-state convection–diffusion equations is a monotone linear stabilization and hence restricted to first order accuracy. From the monotonicity follows that the solutions do not exhibit spurious oscillations. However, due to its low order, the solutions tend to be smeared. The Samarskij upwinding scheme may lose its monotonicity if it is applied to time-dependent convection–diffusion–reaction equations, as in the simulation of precipitation processes, depending on the size of the reactive term, the length of the time step and the numerical quadrature for evaluating the mass matrix. However, it still shows the tendency to smear the numerical solutions.

The SUPG stabilization approach adds a diffusion term to the standard finite element formulation which introduces additional diffusion in streamline direction in a consistent manner. The advantage of using the SUPG stabilization is its higher order accuracy based on superconvergence properties on rectangular meshes. However, its most important drawback is the presence of spurious oscillations at layers of the solutions. An universally applicable higher order method without spurious oscillations does not seem to exist (John and Knobloch, 2007, 2008). In the simulations presented in this paper, undershoots (negative concentrations) were just cut. Overshoots of  $c_A$  and  $c_B$  were also cut, since the maximal values of these concentrations are known by the prescribed inflow concentrations. In contrast, the maximal concentration of  $C$  is known only approximately to be somewhat larger than 1. Without cutting overshoots in  $c_C$ , there were simulations in which the overshoots accumulated and these accumulations finally led to a blow-up of the simulations. We found that cutting the overshoots in  $c_C$  at  $6c_{C,\infty}$  ( $\approx 1.1$  in our simulations) stabilized most of the simulations. This cut-off was applied for all results presented in Section 4.

The equation of the PSD (5) was discretized in time with the forward Euler scheme. Since this equation is convection-dominated, also a stabilized spatial discretization has to be applied. We used the first order sharp upwind finite difference scheme (Roos et al., 1996). The use of this explicit upwind scheme does not require the solution of a linear system of equations for computing the PSD  $f_k$  in  $t_k$  since it leads to a diagonal system matrix.

## 4. Numerical simulations

### 4.1. Setup of the simulations

The population balance system was simulated in the cavity  $\Omega = (0,1)^2$ , see Fig. 1. The size of the inlets is  $1/32$  and the size of the outlet  $1/16$ . The center of the outlet is situated at  $(0.5,0)$ . We studied different positions of the inlets, see Fig. 2.

For the Navier–Stokes equations (1) and (2), parabolic inflow profiles with an integral mean value of 1 (maximal value of 1.5) were applied. Outflow boundary conditions were used at the outlet. The concentrations of the reactants  $A$  at the left inlet and  $B$  at the right inlet were set to 1 for all times. Neumann boundary conditions for these concentrations were used on all other parts of the boundary.

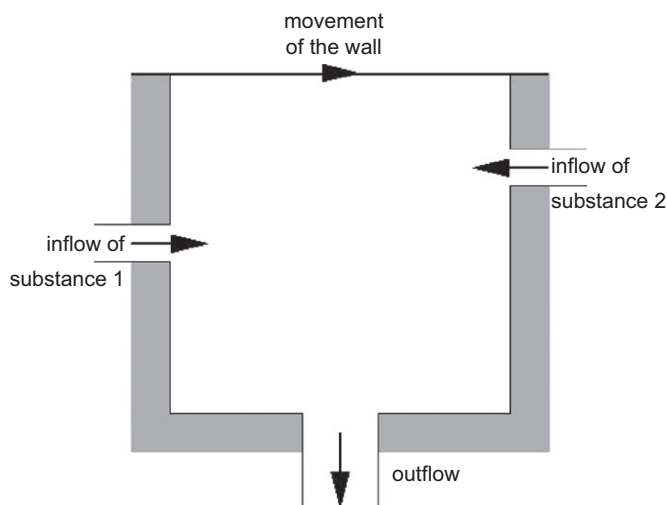


Fig. 1. Cavity with inlets and outlets.

For the substance  $C$ , Neumann boundary conditions were applied on the whole boundary. The boundary condition of the PSD with respect to the smallest internal coordinate was

$$f(t, x_1, x_2, d_{p,\min}) = \frac{B_{\text{nuc}}(c_C)}{f_{\infty} u_{\infty} G(c_C)},$$

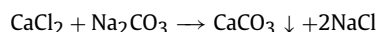
if  $G(c_C) > 0$ . Here,

$$B_{\text{nuc}}(c_C) = k_{\text{nuc}} c_{C,\infty}^5 \max\{0, (c_C - 1)^5\}.$$

Besides the opposite inflows, the mixing of the reactants  $A$  and  $B$  was stimulated by the movement of the upper wall with the velocity  $\mathbf{u}_{\text{drive}} = (u_{1,\text{drive}}/u_{\infty}, 0)^T$ , where we present simulations for  $u_{1,\text{drive}} = u_{\infty}$ .

The initial velocity fields were fully developed flows, computed in a preprocessing step. They are presented in Fig. 2. Initially, the concentrations were zero in  $\Omega$ . The inflow of the reactants started at  $t = 0$ . The initial condition of the PSD was also zero.

In the numerical simulations, the calcium carbonate precipitation



has been considered. The physical and chemical parameters of this process are given by (Tavare and Garside, 1995; Dawe and Zhang, 1996; Chakraborty and Bhatia, 1996; Verdoes et al., 1992):

- $\nu = 10^{-6} \text{ m}^2/\text{s}$ ;
- $\rho = 1 \text{ kg/m}^3$ ;
- $k_G = 10^{-7} \text{ m}^4/(\text{kmol s})$ ;
- $k_{\text{nuc}} = 10^{24} (1/(\text{m}^3 \text{ s})) / (\text{kmol/m}^3)^5$ ;
- $k_R = 10 \text{ m}^3/(\text{kmol s})$ ;
- $c_{C,\infty}^{\text{sat}} = 1.37 \times 10^{-4} \text{ kmol/m}^3$ ;
- $C_2 = 7.2 \times 10^{-9} \text{ m}$ ;
- $C_G = 45.98 \text{ kmol/m}^3$ ;
- $C_{\text{nuc}} = 15.33 \text{ kmol/m}^3$ ;
- $D_A = D_B = D_C = 1.5 \times 10^{-9} \text{ m}^2/\text{s}$ ;
- $\tilde{d}_{p,0} = 10^{-9} \text{ m}$ ; and
- $\tilde{d}_{p,\max} = 10^{-3} \text{ m}$ .

The following reference quantities have been used to derive the dimensionless equations:

- $l_{\infty} = 1 \text{ m}$ ;
- $u_{\infty} = 10^{-3} \text{ m/s}$ ;
- $t_{\infty} = 10^3 \text{ s}$ ;



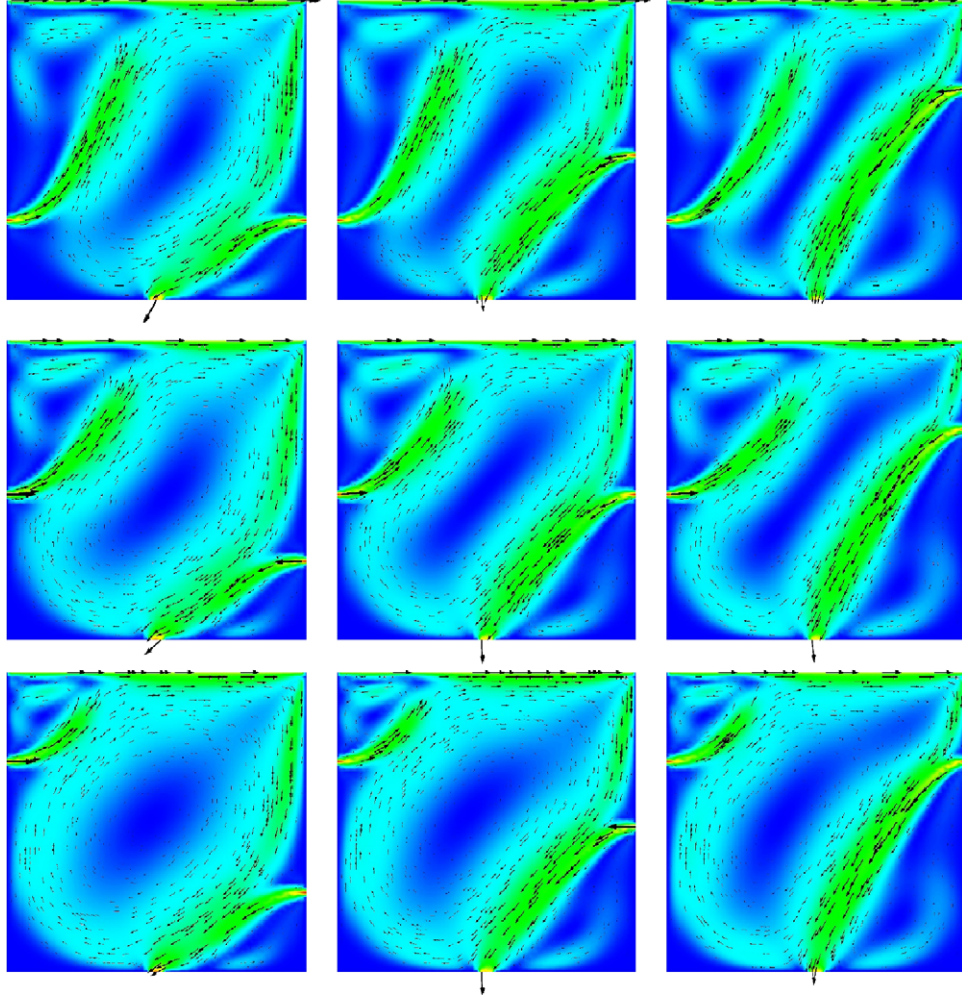


Fig. 2. Fully developed velocity fields for different positions of the inlets.

- $c_\infty = 1 \text{ kmol/m}^3$ ;
- $c_{C,\infty} = 0.183502 \text{ kmol/m}^3$ ;
- $d_{p,\infty} = 10^{-3} \text{ m}$ ; and
- $f_\infty = 2.17486 \times 10^{11} \text{ 1/m}^4$ .

The **Reynolds number** of the flow was  $Re = 1000$ . Considering the equations for computing  $c_i, i \in \{A, B\}$ , and setting the characteristic source in these equations to be  $k_R c_\infty$ , then the **Damköhler number** of the problem is given by

$$Da = \frac{k_R c_\infty l_\infty}{u_\infty} = 10^4.$$

The time stepping schemes were applied with an equidistant time step of length  $\Delta t = 0.0025$ . The velocity field and the concentrations were computed on a  $64 \times 64$  grid consisting of squares. The number of degrees of freedom was 33 282 for the velocity, 12 288 for the pressure and 4225 for each concentration. For the internal coordinate, a non-equidistant grid consisting of 128 layers was used. The grid points were distributed accordingly to the formula

$$1 + (1 - d_{p,\min}) \frac{\tanh(2.75(i/128 - 1))}{\tanh(2.75)},$$

$i = 0, \dots, 128$ . That means, the grid became finer for small particle sizes. The number of nodes for computing the PSD was 545 025.

#### 4.2. Study of different inlet positions

For the driving velocity at the upper wall  $(u_{1,\text{drive}}/u_\infty, 0)^T = (1, 0)^T$ , different positions of the inlets were studied: at the lower part of the lateral walls ( $y \in (8/32, 9/32)$ ), at the middle part ( $y \in (15/32, 16/32)$ ) and at the upper part ( $y \in (22/32, 23/32)$ ). Instantaneous velocity fields for the different situations are presented in Fig. 2. In all flows, a large center vortex and small vortices at the left upper and the right lower corner can be observed.

In the evaluation of the process, the PSD at the center of the outflow  $(0.5, 0)$  was considered. For the representation of the PSD in this point, we used the volume fraction  $q_3$  defined by

$$q_3(\tilde{t}, \tilde{d}_p) := \frac{\tilde{d}_p^3 \tilde{f}(\tilde{t}, 0.5l_\infty, 0, \tilde{d}_p)}{\int_{\tilde{d}_{p,0}}^{\tilde{d}_{p,\max}} \tilde{d}_p^3 \tilde{f}(\tilde{t}, 0.5l_\infty, 0, \tilde{d}_p) d\tilde{d}_p}.$$

The cumulative volume fraction is given by

$$Q_3(\tilde{t}, \tilde{d}_p) := \int_{\tilde{d}_{p,0}}^{\tilde{d}} q_3(\tilde{t}, \tilde{d}_p) d\tilde{d}_p.$$

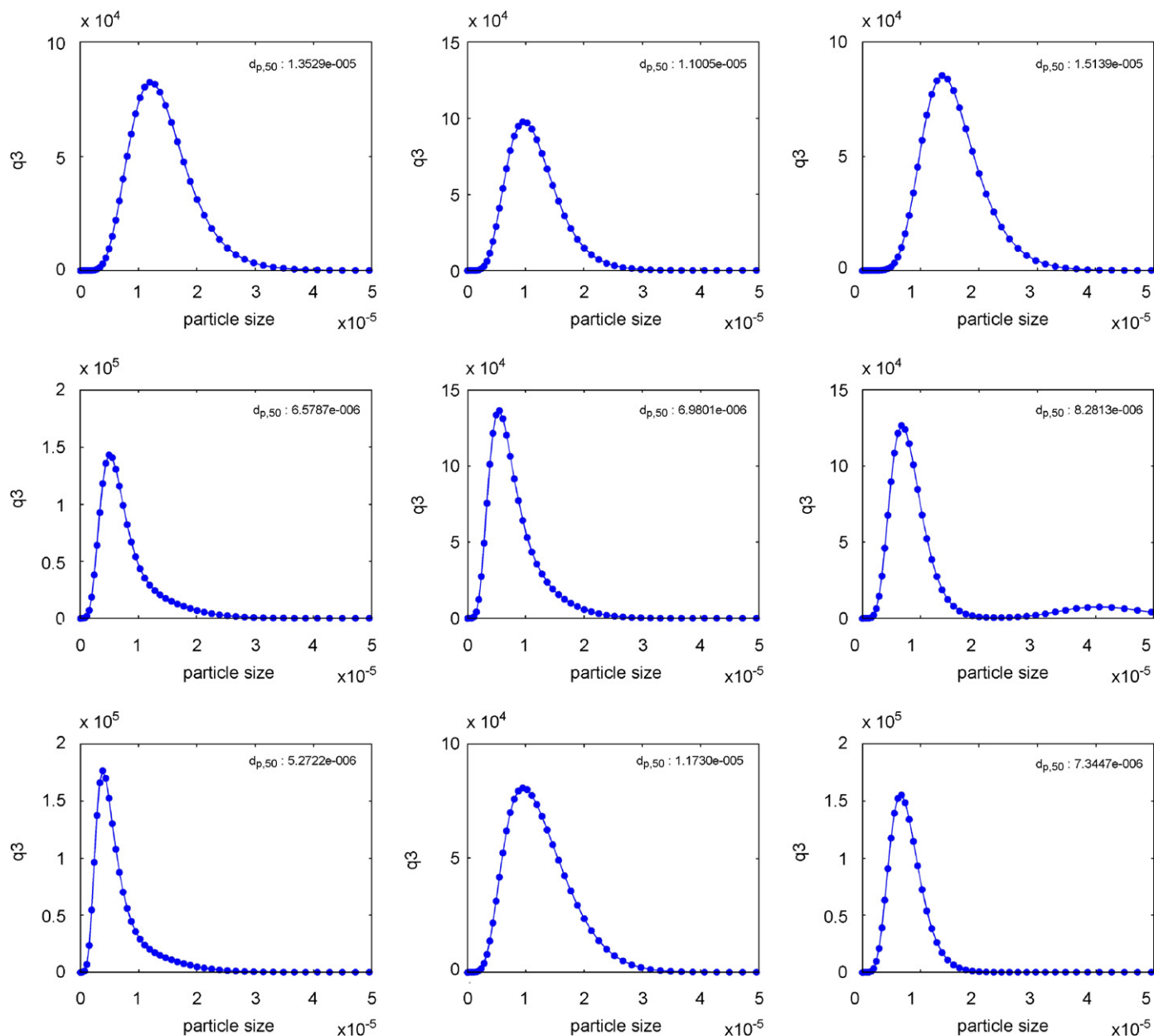


Fig. 3. Volume fractions  $q_3(50000, \tilde{d}_p)$  and medians of the volume fraction for the different positions of the inlets from Fig. 2.

With  $Q_3(\tilde{t}, \tilde{d}_p)$ , the median of the volume fraction  $\tilde{d}_{p,50}(\tilde{t})$  is defined to be the particle size for which  $Q_3(\tilde{t}, \tilde{d}_p)$  takes the value 0.5:

$$\tilde{d}_{p,50}(\tilde{t}) := \{\tilde{d}_p : Q_3(\tilde{t}, \tilde{d}_p) = 0.5\}.$$

The studies with respect to the different inlet positions were carried out with the SUPG finite element stabilization of the convection–diffusion–reaction equations. Fig. 3 shows  $q_3(50000, \tilde{d}_p)$  for the different flow situations from Fig. 2, together with the corresponding medians of the volume fraction. The temporal development of the medians of the volume fraction is presented in Fig. 4.

Two classes of results can be distinguished from Figs. 3 and 4. In the first class, the maximal value of the volume fraction is around  $10^5$  or less and the median of the volume fraction is about  $10^{-5}$ . To this class belong all results obtained with the left inlet at the lower part of the wall. In addition, a result of this class was obtained in the simulation with the left inlet at the upper part of the wall and the

right inlet at the middle part of the wall. The second class of results shows maximal values of the volume fraction which are considerably larger than  $10^5$  and the corresponding medians are considerably less than  $10^{-5}$ . In particular, all simulations with the left inlet at the middle part of the boundary led to results of this class.

The median of the volume fraction is related to the average size of the particles and this size is related to the average residence time of the particles in the domain. As can be seen in Fig. 5, the dissolved  $\text{CaCO}_3$  is situated mostly between the right inlet and the outlet. This is the region where particles nucleate and grow. A large residence time means that the particles do not leave the domain immediately after their nucleation but they pass the outlet, stay in the domain and follow the flow field, for instance along the large center vortex or the small vortex in the right lower corner, and get the opportunity to grow further after reaching again the region between the right inlet and the outlet. This behavior seems to be supported by placing the left inlet at the lower part of the wall.

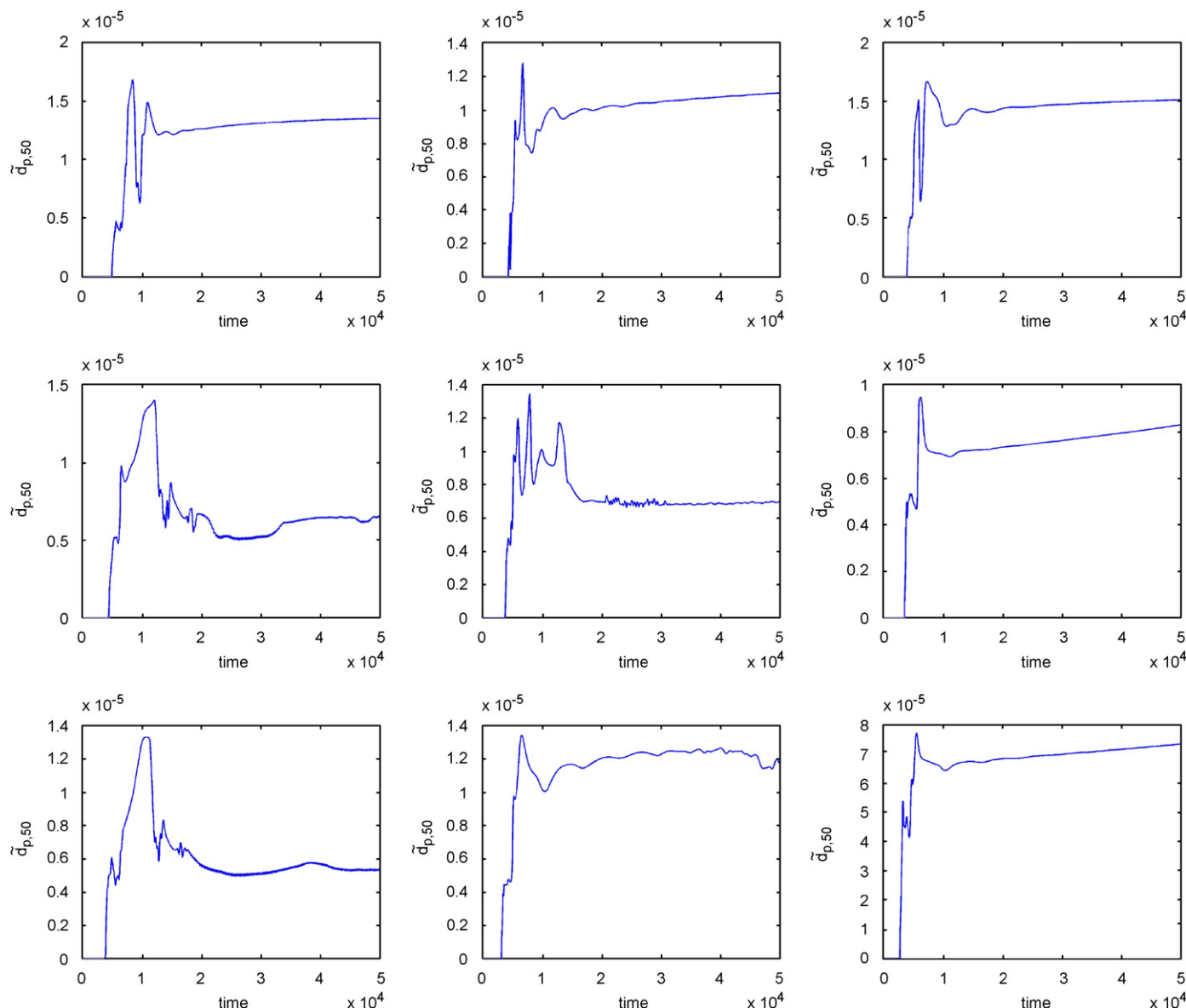


Fig. 4. Temporal development of the medians of the volume fraction for the different positions of the inlets from Fig. 2.

The highest peak of the volume fraction and its smallest median was obtained for the left inlet at the upper part and the right inlet at the lower part of the wall. Placing the inlets vice versa, namely the left one at the lower part and the right one at the upper part, led to the largest median of the volume fraction, which is about three times larger than the smallest one. Remarkable is also a small second peak of the volume fraction at particle size  $4 \times 10^{-5}$  m in the simulation with the left inlet in the middle part and the right inlet at the upper part of the wall.

The nucleation of particles started shortly after the first contact of  $\text{CaCl}_2$  and  $\text{Na}_2\text{CO}_3$ . Depending on the positions of the inlets, the starting time of the nucleation was between 2700 and 4900 s. Then, in all cases, an oscillatory behavior of  $\tilde{d}_{p,50}(\bar{t})$  can be observed, see Fig. 4. After a while, the oscillations ceased and the value of  $\tilde{d}_{p,50}(\bar{t})$  stayed more or less at the same level, generally showing a slight increase. However, there are simulations where some oscillations of  $\tilde{d}_{p,50}(\bar{t})$  can be observed also for later times.

The simulations have been performed on a computer with Intel(R) Xeon(R) X5355 processor with 2.66 GHz. The computation of the

20000 time steps to reach  $\bar{t} = 50000$  took between 123 300 and 134 700 s.

In this first step of our work, we are not yet able to explain all observations in the numerical simulations. Further simulations and the evaluation of more quantities will be necessary to obtain a deeper insight in the precipitation process. The future studies will include also the use of other numerical methods and different grids in order to improve the understanding of the effect of the numerical methods on the computed results.

#### 4.3. Study of different finite element stabilizations of the convection–diffusion–reaction equations

The difference of using the Samarskij upwind scheme and the SUPG method in stabilizing the finite element method of the convection–diffusion–reaction equations can be clearly seen in Fig. 5 for the situation that both inlets are in the middle part of their wall. The smearing of the Samarskij scheme as well as the spurious oscillations of the SUPG scheme are evident.

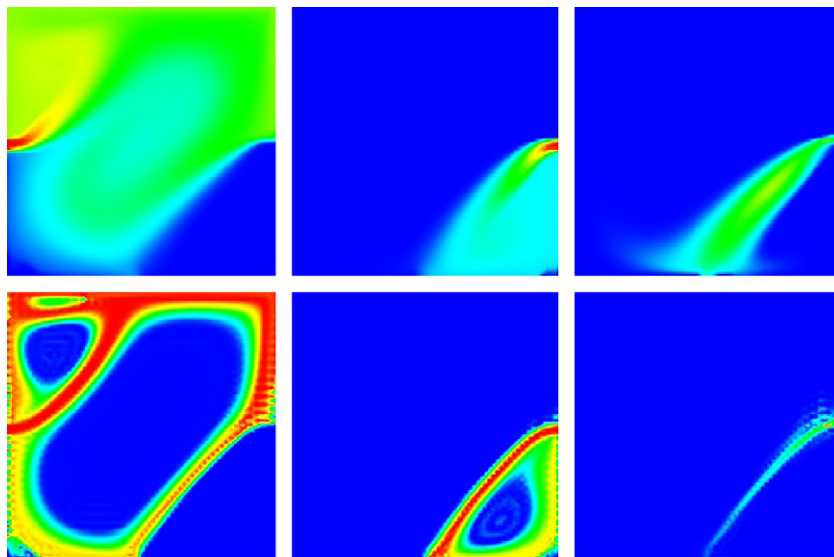


Fig. 5. Concentrations of the dissolved species  $\text{CaCl}_2$ ,  $\text{Na}_2\text{CO}_3$ ,  $\text{CaCO}_3$  (left to right) at  $\tilde{t} = 50\,000$ , top Samarskij upwind stabilization, bottom SUPG stabilization.

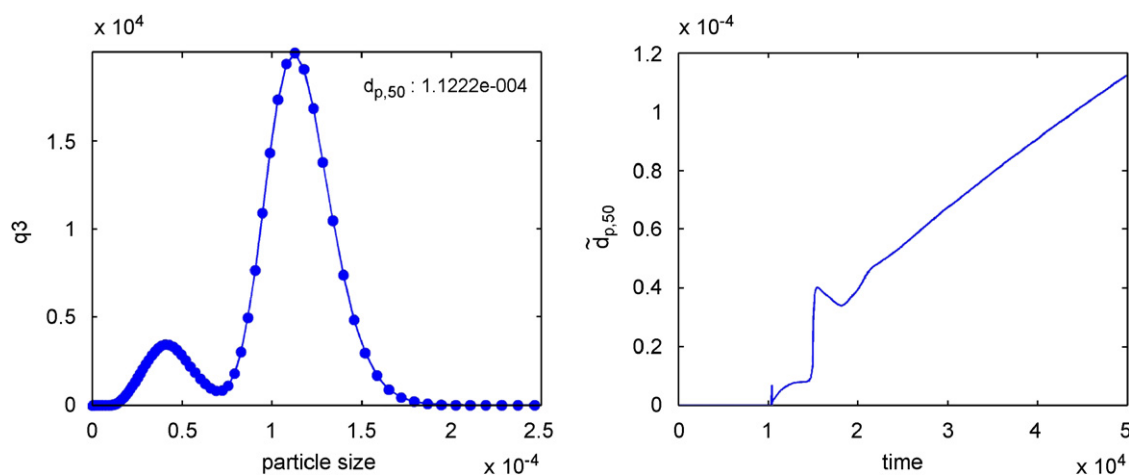


Fig. 6. Volume fraction  $q_3(50\,000, \tilde{d}_p)$  and temporal development of the median of the volume fraction for the simulation with the Samarskij upwind stabilization.

Fig. 6 shows that the smeared solutions of the Samarskij upwind-ing scheme possess a great impact on the volume fraction and its median. The maximal value of the volume fraction is around seven times smaller and the median of the volume fraction is about 16 times larger for the simulation with the Samarskij upwind-ing scheme compared to the SUPG stabilization. In addition, the nucleation of the particles started much later, at around  $10\,400$  s. Then, a continuous (linear) increase can be observed which means that the average size of the particles at the outlet becomes larger and larger. Continuing this simulation, the size will certainly exceed  $\tilde{d}_{p,\max}$ , leading to unphysical results and a useless numerical solution.

The results with the SUPG stabilization correspond much better to our expectations with respect to the average particle size and the distribution of the dissolved species in the domain. However, they are still far from being satisfactory because of the spurious oscillations.

## 5. Conclusion and outlook

The paper presented a numerical approach for simulating the calcium carbonate precipitation in a two-dimensional cavity. The influence of the positions of the inlets on the volume fraction and on

the median of the volume fraction in the center of the outflow were studied. It was shown that the positions have a considerable impact on both quantities. Such effects can be observed only if all equations of the population balance system are simulated without strongly simplifying assumptions like ideal mixing. In a second study, it was demonstrated that the use of the Samarskij upwind finite element stabilization for the convection–diffusion–reaction equations led to completely smeared and useless results.

There will be more than one direction in our future research on the simulation of precipitation processes. The implementation of the numerical solution algorithm to three variables in space is, of course, among them. Turbulent flows, which will occur in applications, will be simulated with the variational multiscale method (John and Kaya, 2005; John and Roland, 2007; John and Kindl, 2008; Bazilevs et al., 2007). A great challenge will be the reduction of the spurious oscillations in the numerical solution for the equations describing the chemical reactions. For instance, schemes presented in John and Knobloch (2007, 2008) will be extended to time-dependent problems. We will also investigate the benefit of algebraic flux correction schemes developed in Kuzmin and Möller (2005) and Kuzmin (2007). A third option is to explore the potential of the recently developed



stabilization based on local projections (Matthies et al., 2007). Concerning the equation for the PSD, implicit temporal discretizations will be used in the future in order to increase the stability and accuracy of the results.

After having identified reliable and accurate numerical schemes, issues like optimal operation and control of precipitation processes can be investigated.

## References

- Bazilevs, Y., Calo, V., Cottrell, J., Hughes, T., Reali, A., Scovazzi, G., 2007. Variational multiscale residual-based turbulence modeling for large eddy simulation of incompressible flows. *Computer Methods in Applied Mechanics and Engineering* 197, 173–201.
- Chakraborty, D., Bhatia, S., 1996. Formation and aggregation of polymorphs in continuous precipitation: 2. Kinetics of  $\text{CaCO}_3$  precipitation. *Industrial & Engineering Chemistry Research* 35, 1995–2006.
- Dawe, R., Zhang, Y., 1996. Kinetics of calcium carbonate scaling using observations from glass micromodels. *Journal of Petroleum Science and Engineering* 18, 179–187.
- Gradl, J., Schwarzer, H.-C., Schwertfirm, F., Manhart, M., Schmid, H.-J., Peukert, W., 2007. Precipitation of nanoparticles in a T-mixer: coupling the particle population dynamics with hydrodynamics through direct numerical simulation. *Chemical Engineering and Processing*, 908–916.
- Heinen, W., Flockerzi, D., Steyer, C., Voigt, A., Sundmacher, K., 2007. Nonlinear dynamics of continuous precipitation reactors: a model based analysis. *Chemical Engineering Science* 62, 4896–4902.
- Hughes, T., Brooks, A., 1979. A multidimensional upwind scheme with no crosswind diffusion. In: Hughes, T. (Ed.), *Finite Element Methods for Convection Dominated Flows*, AMD, vol. 34. ASME, New York, pp. 19–35.
- John, V., 2004. Reference values for drag and lift of a two-dimensional time dependent flow around a cylinder. *International Journal for Numerical Methods in Fluids* 44, 777–788.
- John, V., 2006. On the efficiency of linearization schemes and coupled multigrid methods in the simulation of a 3d flow around a cylinder. *International Journal for Numerical Methods in Fluids* 50, 845–862.
- John, V., Kaya, S., 2005. A finite element variational multiscale method for the Navier–Stokes equations. *SIAM Journal on Scientific Computing* 26, 1485–1503.
- John, V., Kindl, A., 2008. Variants of projection-based finite element variational multiscale methods for the simulation of turbulent flows. *International Journal for Numerical Methods in Fluids* 56, 1321–1328.
- John, V., Knobloch, P., 2007. A comparison of spurious oscillations at layers diminishing (SOLD) methods for convection–diffusion equations: part I—a review. *Computer Methods in Applied Mechanics and Engineering* 196, 2197–2215.
- John, V., Knobloch, P., 2008. A comparison of spurious oscillations at layers diminishing (SOLD) methods for convection–diffusion equations: part II—analysis for  $P_1$  and  $Q_1$  finite elements. *Computer Methods in Applied Mechanics and Engineering* 197, 1997–2014.
- John, V., Roland, M., 2007. Simulations of the turbulent channel flow at  $Re_\tau = 180$  with projection-based finite element variational multiscale methods. *International Journal for Numerical Methods in Fluids* 55, 407–429.
- John, V., Angelov, I., Öncül, A.A., Thévenin, D., 2007. Techniques for the reconstruction of a distribution from a finite number of its moments. *Chemical Engineering Science* 62, 2890–2904.
- Kulikov, V., Briesen, H., Grosch, R., von Wedel, L., Yang, A., Marquardt, W., 2005. Modular dynamic simulation for integrated particulate processes by means of tool integration. *Chemical Engineering Science* 60, 2069–2083.
- Kulikov, V., Briesen, H., Marquardt, W., 2007. A framework for the simulation of mass crystallization considering the effect of fluid dynamics. *Chemical Engineering and Processing* 60, 886–899.
- Kuzmin, D., 2007. Algebraic flux corrections for finite element discretizations of coupled systems. In: *Proceedings of the ECCOMAS Conference Computational Methods for Coupled Problems in Science and Engineering*.
- Kuzmin, D., Möller, M., 2005. Algebraic flux correction I. Scalar conservation laws. In: Kuzmin, R.L.D., Turek, S. (Eds.), *Flux-Corrected Transport: Principles, Algorithms and Applications*. Springer, Berlin, pp. 155–206.
- Lube, G., Rapin, G., 2006. Residual-based stabilized higher-order FEM for advection-dominated problems. *Computer Methods in Applied Mechanics and Engineering* 195, 4124–4138.
- Marchisio, D., Fox, R., 2005. Solution of population balance equations using the direct quadrature method of moments. *Journal of Aerosol Science* 36, 43–73.
- Matthies, G., Tobiska, L., 2002. The inf–sup condition for the mapped  $Q_k/P_{k-1}^{\text{disc}}$  element in arbitrary space dimensions. *Computing* 69, 119–139.
- Matthies, G., Skrzypacz, P., Tobiska, L., 2007. A unified convergence analysis for local projection stabilisations applied to the Oseen problem. *M2AN* 41, 713–742.
- Ramkrishna, D., 2000. *Population Balances: Theory and Applications to Particulate Systems in Engineering*. Academic Press, San Diego.
- Roos, H.-G., Stynes, M., Tobiska, L., 1996. *Numerical Methods for Singularly Perturbed Differential Equations*. Springer, Berlin.
- Schwarzer, H.-C., Schwertfirm, F., Manhart, M., Schmid, H.-J., Peukert, W., 2006. Predictive simulation of nanoparticle precipitation based on the population balance equation. *Chemical Engineering Science* 167–181.
- Tabata, M., 1977. A finite element approximation corresponding to the upwind differencing. *Memoirs of Numerical Mathematics* 1, 47–63.
- Tavare, N., Garside, J., 1995. *Industrial Crystallization: Process Simulation Analysis and Design*, The Plenum Chemical Engineering Series. Plenum Press, New York and London.
- Verdoes, D., Kashchiev, D., van Rosmalen, G., 1992. Determination of nucleation and growth rates from induction times in seeded and unseeded precipitations of calcium carbonate. *Journal of Crystal Growth* 118, 401–413.